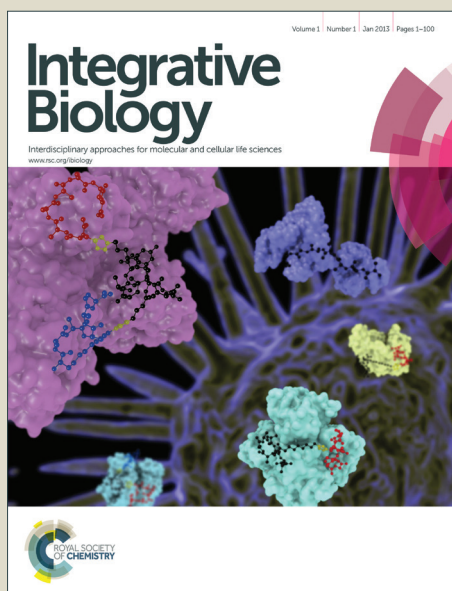


Integrative Biology

Accepted Manuscript



This is an *Accepted Manuscript*, which has been through the Royal Society of Chemistry peer review process and has been accepted for publication.

Accepted Manuscripts are published online shortly after acceptance, before technical editing, formatting and proof reading. Using this free service, authors can make their results available to the community, in citable form, before we publish the edited article. We will replace this *Accepted Manuscript* with the edited and formatted *Advance Article* as soon as it is available.

You can find more information about *Accepted Manuscripts* in the [Information for Authors](#).

Please note that technical editing may introduce minor changes to the text and/or graphics, which may alter content. The journal's standard [Terms & Conditions](#) and the [Ethical guidelines](#) still apply. In no event shall the Royal Society of Chemistry be held responsible for any errors or omissions in this *Accepted Manuscript* or any consequences arising from the use of any information it contains.

ARTICLE

Magnetic engineering of stable rod-shaped stem cell aggregates: circumventing the pitfall of self-bending

Cite this: DOI: 10.1039/x0xx00000x

V. Du,^a D. Fayol,^a M. Reffay,^a N. Luciani,^a J-C. Bacri,^a C. Gay,^a and C. Wilhelm^{a*}Received 00th January 2012,
Accepted 00th January 2012

DOI: 10.1039/x0xx00000x

www.rsc.org/

A current challenge for tissue engineering while restoring the function of diseased or damaged tissue is to customize the tissue according to the target area. Scaffold-free approaches usually yield spheroid shapes with the risk of necrosis at the center due to poor nutrient and oxygen diffusion. Here, we used magnetic forces developed at the cellular scale by miniaturized magnets to create rod-shaped aggregates of stem cells that subsequently matured into a tissue-like structure. However, during the maturation process, the tissue-rods spontaneously bent and coiled into sphere-like structures, triggered by the increasing cell-cell adhesion within the initially non-homogeneous tissue. Optimisation of the intra-tissular magnetic forces successfully hindered the transition, in order to produce stable rod-shaped stem cells aggregates.

Introduction

Current efforts in tissue engineering focus on the assembling of precursor cells into sculpted, differentiated organs or more modestly into therapeutic tissues for in vivo implantation and integration within a damaged organ.

Clever biophysical approaches to making artificial constructs that mimic the structural complexity of native tissues typically use (nano)patterning of the substrate^{1, 2}, but only provide 2D environments and depend on adhesion to the substrate. Cell seeding in a 3D scaffold can be used as an alternative to an extracellular matrix³, and such bioengineered tissues have been successfully implanted in various animal models to restore or improve original tissue functions⁴. However, artificial scaffolds still raise difficult issues of toxicity, degradation, mechanical mismatch and contractility (for cardiac muscle or vascular structures)^{5, 6}. Other techniques have been developed to engineer scaffold-free tissues⁷ composed of cells and the extracellular matrix they produce⁸. Bioprinting⁹⁻¹¹ and cell sheet technology¹² both have the potential to control the geometry of a tissue construct. Magnetic tissue engineering¹³ is a third option to shape a cell assembly, and this strategy of using cells loaded with magnetic nanoparticles to organise them into a tissular structure has been implemented for vascular¹⁴⁻¹⁶,

cardiac^{17, 18}, or skeletal muscle¹⁹ tissue engineering. The magnetic forces combine the advantages of remote action and biological neutrality. Indeed, magnetic labelling with iron oxide nanoparticles doesn't impact stem cell differentiation^{20, 21}, and magnetic labelling can be at use for stem cell tracking²² and targeting²³. More recently, magnetically formed cell spheroids have burst into the scene of tissue engineering^{24, 25}. Suspensions of magnetic cells can indeed be confined in 3D by miniaturized magnets²⁶⁻²⁹. These magnetic spheroids can then be used either as building blocks for a future tissue³⁰⁻³² or as models for studying biophysical 3D cellular interactions^{25, 33}. For all these documented applications, the final spheroid is a spherical aggregate. Rod-shaped replacement tissues would have the advantage of a large interacting surface and good nutrient accessibility, properties that would promote host tissue integration. However, in addition to the technical difficulties of producing 3D rods containing millions of cells, the shape stability of such structures is unexplored. When the contraction capacity of single cells is expressed within a multicellular structure of defined shape, specific stress patterns are generated that affect cell functions such as proliferation^{34, 35} and commitment to a particular differentiation pathway³⁶. For example, increased cell proliferation in high-stress areas has been observed during lung branching^{35, 37}. Cellular forces and

tissue shape are therefore tightly intertwined and a 3D tissular rod-shape may be challenging to maintain.

Here we succeeded to prepare rod-shaped aggregates from individually magnetised stem cells but found that they transitioned into compact spheres after a few hours. We therefore investigated this transition by modulating both cell-to-substrate adhesion and the external magnetic force. We finally succeeded in totally inhibiting the shape transition by maintaining the external magnetic force, thereby obtaining 3D rod-like tissue structures that remained stable for several days.

Results and discussion

Assembly of a million stem cells into a cohesive rod.

Controlled magnetic stress can be exerted on cells composing a tissue aggregate by first inducing them to internalize biologically safe magnetic nanoparticles²⁰ and then submitting them to remote magnetic forces²⁷. Here, mesenchymal stem cells (MSCs) were magnetically labeled in conditions yielding differentiation-capable magnetic stem cells (30 min incubation with 8-nm-diameter maghemite nanoparticles at $[\text{Fe}] = 0.5 \text{ mM}$)²⁰. The resulting intracellular iron mass per cell ($10.5 \pm 0.9 \text{ pg}$) provides each cell with an average magnetic moment of $M_{\text{cell}} = (6.3 \pm 0.5) \cdot 10^{-13} \text{ A} \cdot \text{m}^2$ when submitted to a magnetic field of 0.2 T. A miniaturized soft-iron plate 2 cm long, 1 cm high and $500 \mu\text{m}$ (Fig. 1A) wide was magnetized with a rectangular magnet developing a field strength of 0.2 T. The vertical magnetic gradient developed by the plate ranged from 300 mT/mm in the close vicinity of the magnetic line to 20 mT/mm 1 mm from the line, corresponding to a magnetic force of 200 to 10 pN on each cell (Fig. 1B). The magnetic field is confined close to the line. A million magnetised cells placed in the vicinity of the line formed a rod-like cellular aggregate near-instantly. The aggregate then underwent gradual vertical contraction during the first 10 min, before reaching its initial pseudo-equilibrium shape (height $h_0 = 0.7 \pm 0.2 \text{ mm}$, width $b_0 = 0.8 \pm 0.4 \text{ mm}$, length $L = 11 \pm 1.5 \text{ mm}$, see Fig. 1C).

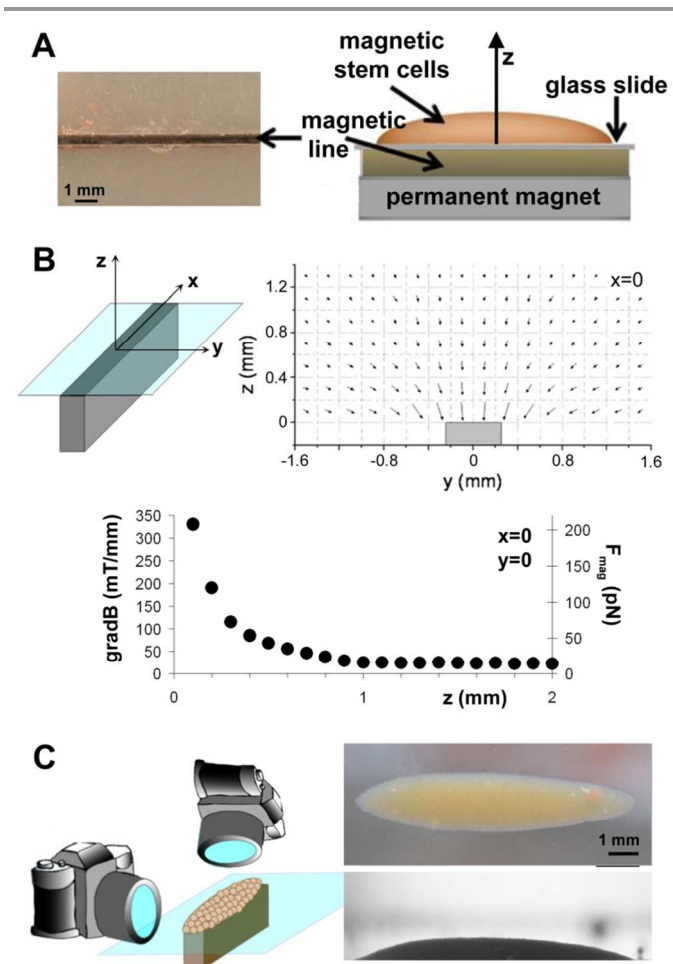


Fig. 1 (A). Schematic representation of the formation of a rod-like aggregate of magnetically labelled stem cells. A thin soft-iron rectangle (photograph taken from the top) is magnetized by a permanent magnet placed underneath it. (B) This magnetized rectangle creates the magnetic field gradient described in the (z, y) map (top). Along z (bottom), it ranges from 250 T/m at the contact point with the glass slide ($100 \mu\text{m}$ above the line) to 20 T/m at 1 mm. The corresponding force (right axis) experienced by a given magnetic cell (10.5 pg of iron per cell) ranges from 200 pN to 10 pN. (C) A typical cellular structure thus formed is shown on the right. The photographs were taken from the top or the side, with an experimental setup involving two cameras with high-magnification objectives.

Rod to sphere shape transition

When the rods were monitored for 30 hours (Fig. 2A), and the initial magnetic force released at the beginning of the experiment (20 min after the rod formation), the rod tips were observed to detach from the substrate after 2.3 ± 0.8 hours (Fig. 2B), meeting after around 15 h. The rod thus transformed first into a ring, and then gradually into a compact sphere after about 30 h.

Asymmetric boundary conditions were first investigated as a possible driver of the observed shape transition, given the presence of the upper free interface. A rod-shaped aggregate was created and then flipped upside-down an hour later with the magnetic field turned off (Fig. 2C). Over the next 15 hours the rod contracted downwards but did not curl up, possibly owing to its weight. However, when the rod was gently detached from the substrate with a flow and was rotated 90° to lie on one side,

it curled up completely in the direction that was upside during the rod formation process (0 - 1 hour). This ruled out any involvement of boundary conditions, as such, in the bending process.

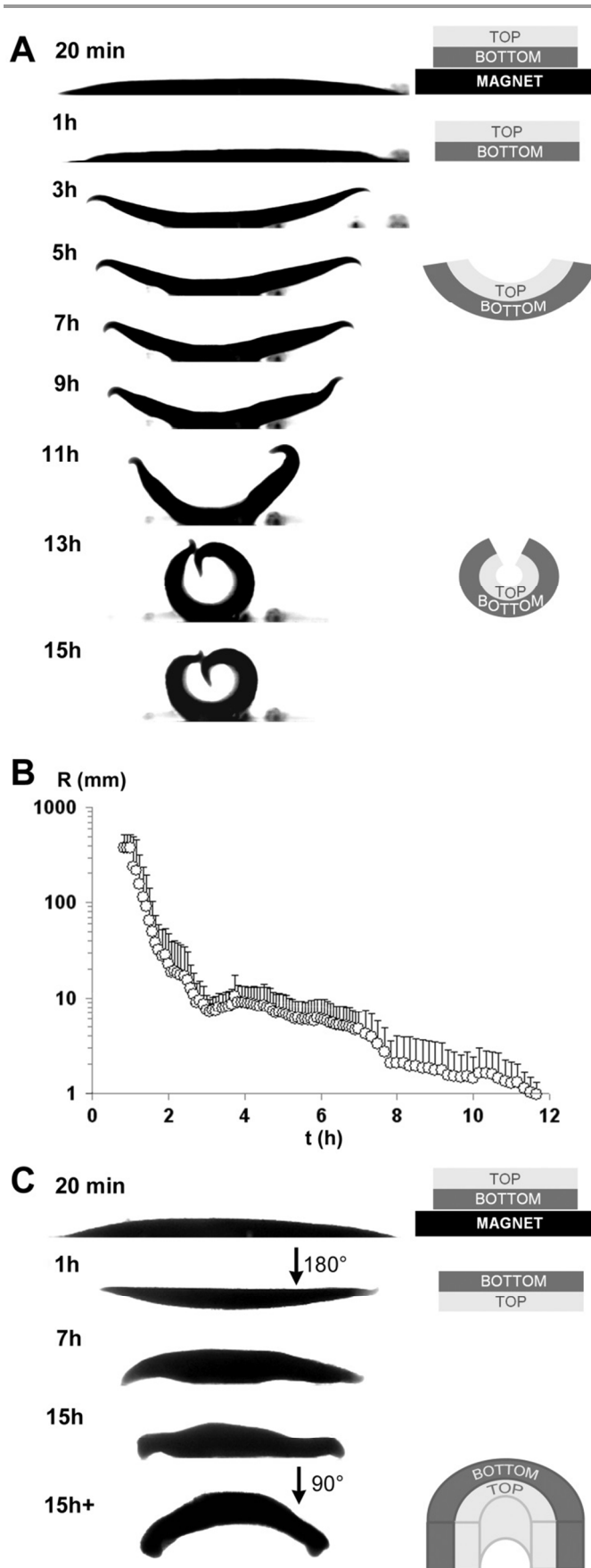


Fig. 2 Observation of the rod-like aggregate. For simplicity, on the right-hand side the rod is represented as a material with two layers: initially, a dark grey layer at the bottom and a light grey layer at the top. (A) The rod-shaped aggregate bends and folds, eventually forming a sphere. The image sequences start at 20 min (immediately after turning off the magnetic field) and continue every two hours from 1 hour until 15 hours. A video is available as electronic supplementary information. (B) The radius of curvature was measured automatically (Matlab) at each time point, then averaged over independent rods (7 samples, error bars represent the standard deviation). It declined from 1 to 3 hours and then remained approximately constant, in the 8 mm range, over the next 5 hours, and finally further transformed to 1-2 mm spherical size. (C) The rod is flipped upside down at $t = 1$ h (gravity unchanged, swapped top and bottom) and the magnetic field is turned off. The bending begins in the direction opposite to the usual direction, at about 15 hours. The rod was then (15h+) turned on its side, through 90°, and immediately bent towards the side that was initially the free interface, as depicted in the right-hand drawing.

Changes in cellular organisation within the rod: a possible driving force for bending

In order to observe the microscopic organization of the cells within the aggregate, first, cell membranes were stained with a red fluorochrome (pkh26) and cell aggregation within the rod was observed in situ, on living cells, by confocal microscopy (Fig. 3A). Twenty minutes after magnetic condensation the cells were found to be packed densely close to the magnetic line and less densely close to the free interface. The same observation was made with rods initially fixed in formalin, then cut (cryosections of 8 μm), and further stained blue for cell nuclei (DAPI) and green for N-cadherin intercellular adhesion proteins (immunostaining) (Fig. 3A for a fixation 20 min after the rod formation, and Fig. 3B for rods fixed 15 h afterwards). At these two time points, the cellular compaction can be quantified by using the cell compacity parameter (or cell volume fraction) $\rho = N_{\text{cell}} V_{\text{cell}} / V_{\text{tot}}$, which ranges from 0 (dilute cells) to 1 (compact aggregate with no intercellular spaces). This compacity ρ was measured as a function of the distance z to the magnet (Fig. 3c). At 20 min, ρ decreased with the distance to the magnet, from 0.8 to 0.67. By contrast, uniform compaction (close to 1) was observed at 15 hours.

Note that after 20 minutes the measured compacity at the free surface of the aggregate (see Fig. 3C) is close to the random close packing compacity of 64%. By contrast, near the solid plate, the compacity reaches 0.8. Correspondingly, cells are almost spherical near the free surface and more faceted near the solid plate (see Fig. 3A). The reason for the initial gradient in compacity is that the magnetic force plays the same role as gravity in a liquid: all cells are attracted towards the magnet, hence the cells in the lower part of the aggregate are under higher pressure due to the cells above them.

As a result, the lower cells are squeezed against each other and are faceted, which explains the high compacity. Comparatively, the cells near the free surface are more round, hence the lower compacity. As time proceeds, neighbouring cells adhere more³³. As can be seen in Figure 3A, this does not alter the typical cell volume but only the free space between the cells. In other words, cell-cell adhesion generates a decrease in the aggregate volume. The aggregate eventually reaches maximum compacity (see Figure 3A), whether the initial compacity was

low or already quite high. In other words, the local volume decrease is stronger in the upper part (which was initially less compact) and weaker in the lower part (which was initially quite dense). Because the upper part contracts more than the lower part, the overall rod shape is bent upwards when it is able to detach from the solid surface. In the meantime, the volume contraction that results from cell-cell adhesion competes with the attachment to the substrate. Hence, longitudinal tensile (stretching) stresses develop in the aggregate (they are stronger in the upper part) and the overall aggregate thickness is reduced (compare Figure 2A at 20 min and 1h). As long as the aggregate adheres, the tensile stresses are balanced by horizontal (adhesion) forces between the rod and the substrate, especially near each end of the rod. These adhesion forces and the elastic energy stored in the whole aggregate are the driving force for the detachment of the aggregate from the substrate.

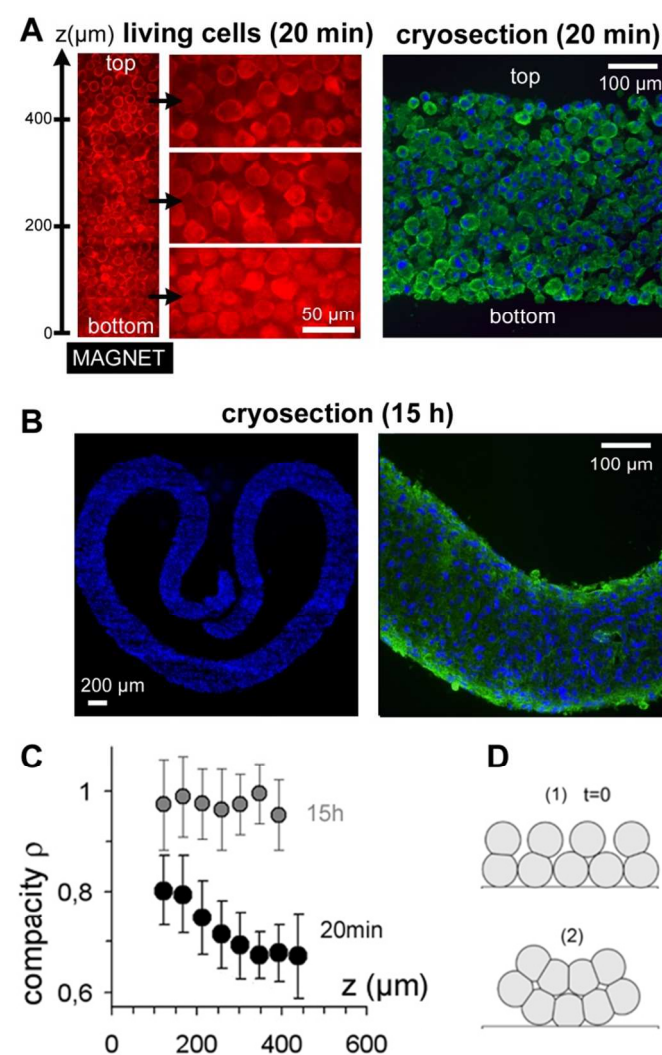


Fig. 3 (A) Left: In situ observation of the compaction of a live cell aggregate created by magnetic attraction, after cell membrane staining with the red fluorescent molecule pkh26: cells are more compacted when closer to the magnet ($z=0$). Right: Rod-shaped aggregates were also fixed 20 min after their formation, and then cut into 8- μm slices after fixation in formalin and inclusion

in OCT, in order to determine cell compacity layer by layer. The cell nuclei are labelled blue (DAPI) and the intercellular adhesion molecules (E-cadherins) green (revealing the cell membranes). (B) Cryosections of rods fixed 15 h after their formation (4x magnification on the left, only DAPI staining; 20x magnification on the right, superposition of DAPI and E-cadherin staining). (C) Variation of the measured ($\rho(20\text{ min})$, $\rho(15\text{h})$) compacities as a function of the distance from the magnetic line. (D) Scheme of the spontaneous bending of a cellular rod. The rod initially consists of layers of cells of unequal compacity (top drawing). In the following hours, the cells adhere to one another and the aggregate reaches near maximum compacity in all layers. As a result, because the upper layer was initially less dense, its length after detachment is shorter. Correspondingly, the rod is bent (bottom drawing).

The actual detachment should also depend on the strength of adhesion (which prevents horizontal aggregate retraction) and on the presence or absence of a continued applied magnetic force (which hinders bending).

We expect the complex mechanical history of the present rod aggregates to be somewhat more general: (i) tensile forces are to be expected in the presence of adhesion to any substrate that is more rigid than the aggregate, and (ii) bending should occur in all situations where an external body force is exerted within the forming aggregate and thus generates a compacity gradient.

Preventing the bending process

Although adhesion between cells is desired in order to yield a cohesive aggregate suitable for tissue engineering and implant, the associated early detachment and bending need to be circumvented. We tried to prevent them bending by applying the magnetic force for a longer time or by enhancing cell adhesion to the substrate. The time at which the rod tips detached from the substrate was considered as a characteristic time in the bending dynamics. Indeed, this event corresponds to the situation where the force developed as a result of the aggregate contraction overcomes both the cell adhesion to the substrate and the magnetic force. The characteristic time of rod detachment was 2.3 ± 0.8 h when no magnetic force was applied after rod formation and when the surface of the substrate was left untreated.

We increased the adhesion of the first cell layer to the substrate by saturating the glass surface with a fibronectin coating. Under these conditions the rod tips no longer detached during the 30-hour observation period (Fig. 4a). However, when cell-to-substrate adhesion was artificially broken by applying a rapid flow, the rod tips detached immediately and the rod adopted a curved shape. When the rods were observed daily for up to 10 days in the incubator (without the camera setup), bending was found to occur between day 3 and day 4 (72 h and 96 h after rod formation), but this time a thin layer of cells remained attached to the substrate, evidencing some kind of tearing of the rod parallel to the adhesive substrate (Fig. 4b).

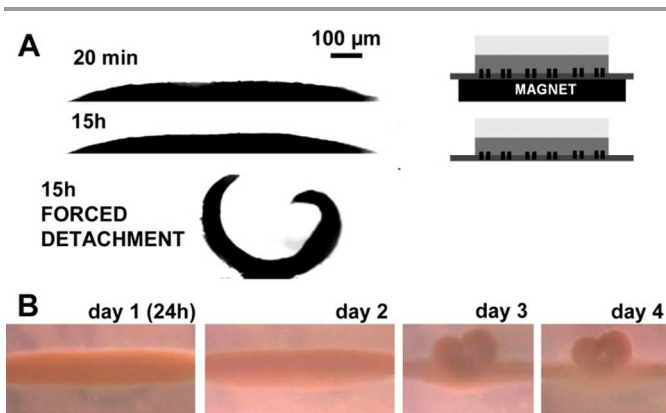


Fig. 4 Effect of enhanced cell-to-substrate adhesion. A. With strong cell-to-substrate adhesion ensured by a fibronectin coating ($50\ \mu\text{g}/\text{ml}$ for 1 h), the cells remain attached to the substrate 15 hours after rod formation. Contraction and bending occur immediately when the adhesive bonds to the substrate are broken externally (bottom image, forced detachment). Bar= $100\ \mu\text{m}$. B. When the rod is further matured in an incubator for a few days, it starts to bend approximately 3 days after seeding on the fibronectin-coated surface, despite the enhanced adhesion. The rod detachment then leaves a thin layer of cells still attached to the substrate (see image at day 4). The bulk of the tissue eventually adopts a spherical shape.

Beside enhanced adhesion, another potential way to prevent this bending was to maintain the applied magnetic field after rod formation, thereby pressing the rod against the substrate. Under these conditions, bending was indeed delayed, though not blocked: tips detached after 11.2 ± 2.7 h (Fig. 5a). Interestingly, the rod bent sharply and quickly, with radii of curvature in the 1-mm range (Fig. 5b) without resting at intermediate curvatures like in the absence of magnetic field (see Fig. 2b). This 1-mm radius of curvature is thus similar whether or not the magnetic force is maintained from 20 minutes to the end of the experiment, many hours later. If the magnetic field and enhanced adhesion was combined, the exact same behaviour as in Fig. 4 was observed.

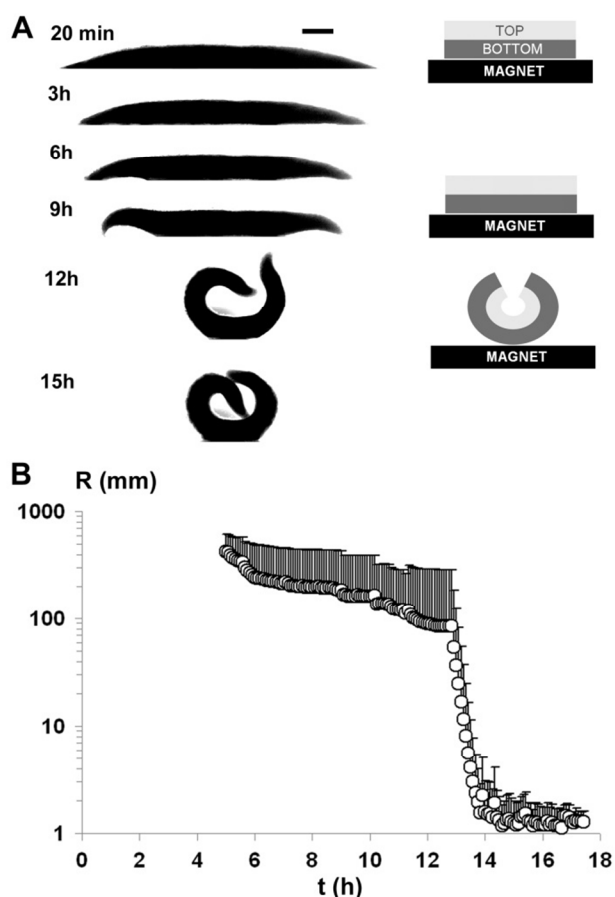


Fig. 5 Effect of the magnetic field. **A.** When a magnetic force is permanently applied to the cell bodies (ranging from 700 pN at the substrate surface to 100 pN in the upper cell layer, the tips detach at 10 ± 1.4 h. Bar=100 μ m. A video is available as electronic supplementary information. **B.** The measured radius of curvature R is averaged for 6 independent rods (error bars represent the standard deviation) in the magnetic compression condition, demonstrating that sharp bending occurs after 10 hours.

In summary, keeping the applied magnetic force or enhancing the adhesion to the substrate by suitable coating was inefficient at preventing rod bending, whether after adhesive detachment or after cohesive failure. In other words, as the cell-cell adhesion bonds mature and the cells progress along their differentiation pathway, the tensile stresses within the aggregate continue to increase and eventually overcome either the adhesive bonds to the substrate or the toughness of some of the weaker cells within the aggregate.

Preventing bending by increasing the magnetic force: production of stable tissue rods

The last solution to prevent bending and thereby create a stable tissue rod was to further increase the applied magnetic force. To do so, the magnetic device was changed once the line had been formed. Small cylindrical permanent neodymium magnets (diameter 3 mm, height 6 mm) developing a strong magnetic field at their surface (550 mT) were used in combinations of two or four. The magnetic field gradient in the region 1 mm above the magnets ranged between 700 and 300 mT/mm

(Fig. 6a), values 10 times higher than those created by the initial magnetized line, and developing a force of between 200 and 500 pN on each cell.

As detachment began at the extremities of the rod, we first placed one magnet at each end. When these magnets were placed beyond the rod extremities (to exert a restoring torque only on the rod tips), the force was not sufficient to prevent bending (Fig. 6b). When the magnets were placed just below the rod extremities, the magnetic force was strong enough to prevent bending but also attracted the cells located in the centre, resulting in rod fracture (Fig. 6c). We thus suppressed this lateral force by arranging a line of 4 magnets with no spacing between them and spanning the entire length of the rod (Fig. 6d). This 4 magnets configuration allowed the tissue to retain its rod shape, with no bending and no fracture.

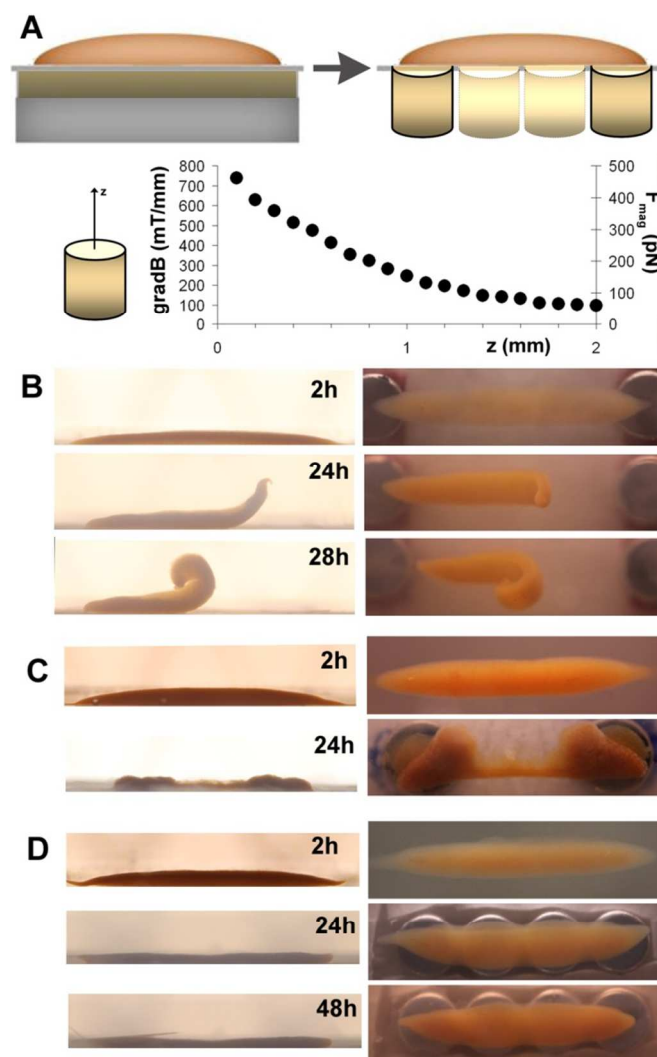


Fig. 6 New magnetic field devices. **A.** After rod formation with the rectangular magnetic plate used previously, the rod was placed over small cylindrical magnets (diameter 3 mm) developing a strong magnetic field gradient (in the range of 100 T/m 2 mm from the magnet surface to 800 T/m at 0.1 mm). The corresponding magnetic force, shown on the right-hand vertical axis, is significantly stronger than the earlier one shown on Fig. 1b. We either placed two magnets at different distances from the rod tips, or four magnets in a line with no spaces between them. **B.** With one magnet at each end of the rod, the

force was not enough to prevent bending, which occurred 24h after rod formation. C. By contrast, when the two magnets were placed just below the rod tips, the lateral attractive force was sufficient to fracture the rod half-way between both magnets. D. With four magnets aligned with no spaces between them, and spanning the entire length of the rod, the rod shape was maintained, with no bending.

No bending occurred after 7 days when 4 aligned magnets were used, and the rod shape was maintained for up to 2 weeks. The resulting rods could easily be manipulated with tweezers (Fig. 7a). Thin cryosections of these rods were immunostained for E-cadherins, and nuclei. Merged images are shown in Fig. 7b, demonstrating a highly cohesive cellular structure, in a rod-like shape. For comparison, images of cells aggregated by centrifugation (same number of cells: 1 million) and kept in the incubator for one week are shown in Fig. 7c: the structure thus obtained was totally loose, with no cell-cell adhesion.

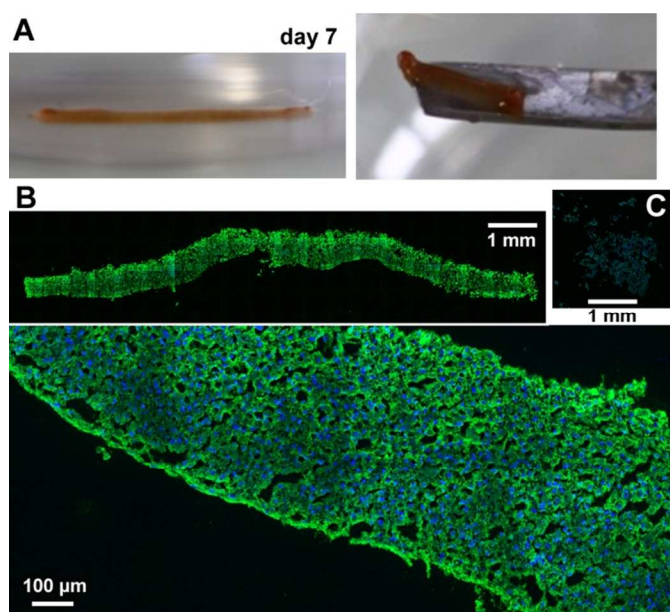


Fig. 7 Images of a rod-shaped aggregate 7 days after its formation. A. This tissue-like structure was easily manipulated with tweezers. B. Staining of cryosections (E-cadherin in red, nuclei in blue) demonstrates a cohesive structure with dense cell-cell adhesion. C. By contrast, the control aggregate of 1 million stem cells (same number as for the rod) formed by centrifugation has a loose structure with no cell-cell adhesion.

Conclusions

Herein, we developed an original method to pattern a 3D rod-shaped piece of tissue using miniaturized magnets. As compared to a spherical geometry, the high surface area-to-volume ratio of a rod relative to a sphere facilitates the diffusion of oxygen and nutrients. It may also enhance integration with damaged tissues *in vivo*.

The first observation was that the engineered rod bended, and transitioned to a sphere in less than 12h, due to the initial gradient in cell organization (compactness) within the rod. Such gradients in cell packing are expected to appear in any tissue engineered

under the application of an external body force. This finding should thus assist with the engineering of stem cell aggregates that have a permanent rod shape and may be particularly suited to therapeutic applications. However, this self-bending can be circumvented by tuning the applied force: we succeeded in maintaining a 3D, scaffold-free, rod-shaped (rather than sheet-shaped) tissue of 1 million cells (or more) with no observed necrosis during several days and which can be manipulated easily.

Experimental section

Cell culture and labelling

Human mesenchymal stem cells (MSC, Lonza) were maintained in a undifferentiated state and cultured in T75 flasks in MSCBM medium (Lonza, PT-3238) supplemented with MSCGM SingleQuot (Lonza, PT-4105). At 80% confluence, the cells were rinsed with 15 ml of RPMI 1640 medium and then incubated for 30 min at 37°C with 5% CO₂ in RPMI 1640 supplemented with 0.5 mM citrate-coated iron oxide magnetic nanoparticles (8 nm diameter) and 5 mM citrate to prevent nanoparticle aggregation. The cells were then washed with 15 ml of RPMI and incubated overnight in complete MSCGM medium. Prior to use, the cells were detached (trypsin) and resuspended in a medium favoring cell-cell adhesion and tissue formation (further called aggregation medium), consisting of DMEM high glucose with Glutamax (Gibco #61956-026) supplemented with 0.1 µM dexamethasone, 1 mM sodium pyruvate, 50 µM ascorbic acid-2 phosphate, 0.35 µM L-proline, 1X penicillin/streptomycin and 1X ITS+Premix (BD Biosciences #354352), and 0.04 µg/ml TGF-β3 (Fitzerald #A13032813).

Magnetophoresis

The per-cell nanoparticle content was quantified by magnetophoresis²⁰. Briefly, it consists in measuring the velocity of single cells (v_{cell}) towards a magnet developing a uniform magnetic field gradient ($\text{grad}B=17 \text{ T/m}$, $B=45\text{mT}$). Then, by equaling the corresponding cellular magnetic force ($M_{\text{cell}} \times \text{grad}B$, M_{cell} being the cell magnetic moment), and the viscous drag ($6\pi\eta R_{\text{cell}} v_{\text{cell}}$, with η the water viscosity and R_{cell} the cell radius), one obtains the cell magnetisation M_{cell} (expressed in $\text{A}\cdot\text{m}^2$), or equivalently the mass of iron per-cell (in a 45mT field, $6.5 \times 10^{-14} \text{A}\cdot\text{m}^2$ equals 1pg of iron). Practically, single cell velocity was determined by videomicroscopy over a minimum population of 100 cells.

Magnetic devices

For rod-shaped tissue formation, a rectangular piece of soft iron (length 2 cm, height 1 cm, width 0.5 mm) was magnetized with a permanent magnet (rectangular: 1 cm × 4 mm × 10 cm) and placed underneath the dish. For rod-shaped maintenance, a linear array of small cylindrical magnets (diameter 3 mm, height 6 mm) was used to increase the magnetic attraction. The magnetic gradients were measured by tracking the motion of

18- μm -diameter magnetic beads towards the magnetized linear attractor or towards the cylindrical magnet. Balancing the viscous force ($6\pi\eta Rv$, where η is the medium viscosity, $R=6\ \mu\text{m}$ the bead diameter, and v the calculated velocity) with the magnetic force ($M\text{grad}B$) directly yields the magnetic gradient $\text{grad}B$ exerted by the attractors. The force then experienced by the cells is easily calculated as $M_{\text{cell}}\times\text{grad}B$, with M_{cell} the magnetic moment provided by the internalised magnetic nanoparticles, and measured by single cell magnetophoresis, as previously described.

Rod formation

Magnetically labelled MSCs were trypsinized, diluted in the aggregation medium, and centrifuged to obtain a pellet of 1 million cells. The pellet was resuspended in 50 μl and dropped into a glass-bottomed Petri dish containing 3 mL of medium, over the magnetic line device. For adhesion experiments the Petri dish was first coated with fibronectin diluted to 50 $\mu\text{g}/\text{ml}$ in PBS, for 1 h. The rods thus obtained were placed either in a CO₂ incubator at 37°C with medium changes every 3 days, or on a 37°C thermalized stage for observation with a Canon EOS 50D camera equipped with a Canon EF 100 mm macro lens. Medium was changed every 2 days with fresh aggregation medium.

Cell staining

Aggregates were fixed with 10% formalin, frozen in liquid nitrogen, and cryosectioned (8 μm). BSA 1% was used to block non specific protein binding sites. The cryosections were incubated with monoclonal antibodies against E-cadherin (Sigma) at 1:1000, then washed and incubated with secondary anti-rabbit antibody at 1:500. The cell nuclei were stained with Dapi (Invitrogen) at 1:2000. Stained cells were observed by confocal microscopy.

Acknowledgements

This work was supported by the French Research Funding Agency (Agence Nationale de la Recherche, ANR) within the framework of the MagStem project (ANR-11 SVSE5).

Notes and references

^a Laboratoire Matière et Systèmes Complexes, CNRS UMR 7057, Université Paris 7, France.

* claire.wilhelm@univ-paris-diderot.fr

- H. N. Kim, A. Jiao, N. S. Hwang, M. S. Kim, D. H. Kang, D.-H. Kim and K.-Y. Suh, *Advanced drug delivery reviews*, 2013, **65**, 536-558.
- D.-H. Kim, E. A. Lipke, P. Kim, R. Cheong, S. Thompson, M. Delannoy, K.-Y. Suh, L. Tung and A. Levchenko, *Proceedings of the National Academy of Sciences*, 2010, **107**, 565-570.
- J. S. Miller, K. R. Stevens, M. T. Yang, B. M. Baker, D.-H. T. Nguyen, D. M. Cohen, E. Toro, A. A. Chen, P. A. Galie, X. Yu, R. Chaturvedi, S. N. Bhatia and C. S. Chen, *Nat Mater*, 2012, **11**, 768-774.
- W.-H. Zimmermann, I. Melnychenko, G. Wasmeier, M. Didié, H. Naito, U. Nixdorff, A. Hess, L. Budinsky, K. Brune and B. Michaelis, *Nature medicine*, 2006, **12**, 452-458.
- D. F. Williams, *Biomaterials*, 2008, **29**, 2941-2953.
- B. Chan and K. Leong, *Eur. Spine J.*, 2008, **17**, 467-479.
- J. M. Kelm and M. Fussenegger, *Trends in biotechnology*, **22**, 195-202.
- W. R. Legant, A. Pathak, M. T. Yang, V. S. Deshpande, R. M. McMeeking and C. S. Chen, *Proceedings of the National Academy of Sciences*, 2009, **106**, 10097-10102.
- U. Demirci and G. Montesano, *Lab on a chip*, 2007, **7**, 1139-1145.
- K. Jakab, C. Norotte, B. Damon, F. Marga, A. Neagu, C. L. Besch-Williford, A. Kachurin, K. H. Church, H. Park and V. Mironov, *Tissue Engineering Part A*, 2008, **14**, 413-421.
- C. Norotte, F. S. Marga, L. E. Niklason and G. Forgacs, *Biomaterials*, 2009, **30**, 5910-5917.
- K. Sakaguchi, T. Shimizu, S. Horaguchi, H. Sekine, M. Yamato, M. Umezumi and T. Okano, *Scientific reports*, 2013, **3**.
- A. Ito and M. Kamihira, in *Progress in molecular biology and translational science*, 2011, vol. 104, pp. 355-395.
- J. Gonzalez-Molina, J. Riegler, P. Southern, D. Ortega, C. Frangos, Y. Angelopoulos, S. Husain, M. Lythgoe, Q. Pankhurst and R. Day, *Journal of The Royal Society Interface*, 2012, rsif20120316.
- D. Fayol, C. Le Visage, J. Ino, F. Gazeau, D. Letourneur and C. Wilhelm, *Cell transplantation*, 2013, **22**, 2105-2118.
- A. Ito, K. Ino, M. Hayashida, T. Kobayashi, H. Matsunuma, H. Kagami, M. Ueda and H. Honda, *Tissue Eng.*, 2005, **11**, 1553-1561.
- H. Akiyama, A. Ito, M. Sato, Y. Kawabe and M. Kamihira, *International Journal of Molecular Sciences*, 2010, **11**, 2910-2920.
- K. Shimizu, A. Ito, J. K. Lee, T. Yoshida, K. Miwa, H. Ishiguro, Y. Numaguchi, T. Murohara, I. Kodama and H. Honda, *Biotechnol. Bioeng.*, 2007, **96**, 803-809.
- Y. Yamamoto, A. Ito, H. Fujita, E. Nagamori, Y. Kawabe and M. Kamihira, *Tissue Engineering - Part A*, 2011, **17**, 107-114.
- D. Fayol, N. Luciani, L. Lartigue, F. Gazeau and C. Wilhelm, *Advanced healthcare materials*, 2013, **2**, 313-325.
- H. Markides, M. Rotherham and A. J. El Haj, *Journal of Nanomaterials*, 2012, **2012**.
- H. Markides, O. Kehoe, R. H. Morris and A. J. El Haj, *Stem Cell Research and Therapy*, 2013, **4**.
- A. J. El Haj, J. R. Glossop, H. S. Sura, M. R. Lees, B. Hu, S. Wolbank, M. van Griensven, H. Redl and J. Dobson, *Journal of Tissue Engineering and Regenerative Medicine*, 2012.
- L. Yu, M. C. Chen and K. C. Cheung, *Lab on a chip*, 2010, **10**, 2424-2432.
- A. M. Bratt-Leal, K. L. Kepple, R. L. Carpenedo, M. T. Cooke and T. C. McDevitt, *Integrative Biology*, 2011, **3**, 1224-1232.
- K. Ino, M. Okochi, N. Konishi, M. Nakatochi, R. Imai, M. Shikida, A. Ito and H. Honda, *Lab on a Chip - Miniaturisation for Chemistry and Biology*, 2007, **8**, 134-142.
- G. Frasca, F. Gazeau and C. Wilhelm, *Langmuir*, 2009, **25**, 2348-2354.

Journal Name

28. W. Liu, Y. Li, S. Feng, J. Ning, J. Wang, M. Gou, H. Chen, F. Xu and Y. Du, *Lab on a chip*, 2014.
29. J. A. Kim, J.-H. Choi, M. Kim, W. J. Rhee, B. Son, H.-K. Jung and T. H. Park, *Biomaterials*, 2013, **34**, 8555-8563.
30. B. R. Whatley, X. Li, N. Zhang and X. Wen, *Journal of Biomedical Materials Research Part A*, 2014, **102**, 1537-1547.
31. B. M. Mattix, T. R. Olsen, M. Casco, L. Reese, J. T. Poole, J. Zhang, R. P. Visconti, A. Simionescu, D. T. Simionescu and F. Alexis, *Biomaterials*, 2014, **35**, 949-960.
32. D. Fayol, G. Frasca, C. Le Visage, F. Gazeau, N. Luciani and C. Wilhelm, *Advanced Materials*, 2013, **25**, 2611-2616.
33. G. Frasca, V. Du, J. C. Bacri, F. Gazeau, C. Gay and C. Wilhelm, *Soft Matter*, 2014, **10**, 5045-5054.
34. C. M. Nelson, R. P. Jean, J. L. Tan, W. F. Liu, N. J. Sniadecki, A. A. Spector and C. S. Chen, *Proc. Natl. Acad. Sci. U. S. A.*, 2005, **102**, 11594-11599.
35. C. M. Nelson, M. M. VanDuijn, J. L. Inman, D. A. Fletcher and M. J. Bissell, *Science*, 2006, **314**, 298-300.
36. S. A. Ruiz and C. S. Chen, *Stem Cells*, 2008, **26**, 2921-2927.
37. K. A. Moore, T. Polte, S. Huang, B. Shi, E. Alsberg, M. E. Sunday and D. E. Ingber, *Dev. Dyn.*, 2005, **232**, 268-281.